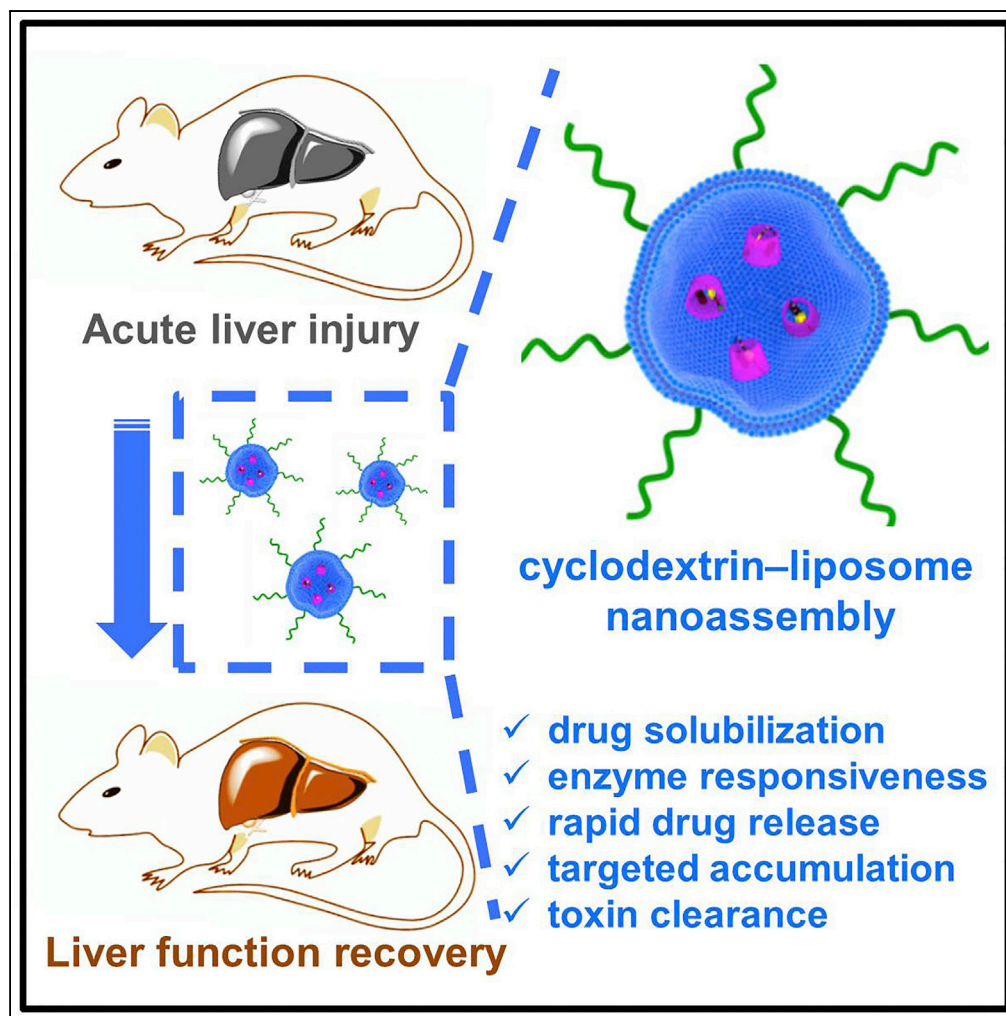


Article

Drug Displacement Strategy for Treatment of Acute Liver Injury with Cyclodextrin-Liposome Nanoassembly



Ying-Ming Zhang,
Xun Xu, Qilin Yu,
Hua-Jiang Yu, Yu
Liu

yuliu@nankai.edu.cn

HIGHLIGHTS

Drug displacement strategy is presented for treatment of acute liver injury

Ternary supramolecular assembly specifically accumulates in the liver of mice

Drug release is triggered by the overexpression of alkaline phosphatase

Clearance of bile acids and recovery of liver function are simultaneously realized

Zhang et al., iScience 15, 223–233
May 31, 2019 © 2019 The Author(s).
<https://doi.org/10.1016/j.isci.2019.04.029>

Article

Drug Displacement Strategy for Treatment of Acute Liver Injury with Cyclodextrin-Liposome Nanoassembly

Ying-Ming Zhang,¹ Xun Xu,¹ Qilin Yu,¹ Hua-Jiang Yu,¹ and Yu Liu^{1,2,3,*}

SUMMARY

Biofunctional supramolecular assemblies that combine macrocyclic receptors and amphiphiles are potent drug delivery systems, but optimization and implementation challenges remain. We herein describe a cooperative drug displacement strategy exemplified by the use of cyclodextrin-liposome supramolecular nanoassemblies as a therapy for acute liver injury. The hepatoprotective drug silibinin was solubilized in phosphotyramine-modified β -cyclodextrin, and subsequent encapsulation of the silibinin-cyclodextrin complex in phosphatidylcholine liposomes gave uniformly sized and stable nanoassemblies that accumulated preferentially in the liver of mice. Enzymatic cleavage of the phosphate ester of the β -cyclodextrin resulted in rapid release of the encapsulated silibinin. Significantly, silibinin could be readily displaced by cytotoxic bile acids, thus leading to the removal of excess bile acids from the bodies of mice and the recovery of liver function. Our results demonstrate that cyclodextrin-based nanoassemblies with a dual role of solubilizing a drug and removing toxins constitute a promising therapy for hepatic injury.

INTRODUCTION

The use of artificial supramolecular nanoassemblies as drug carriers can circumvent major hurdles associated with the delivery of drug molecules to their sites of action (Cheng et al., 2019; Pugliese et al., 2018; Kitagishi and Minegishi, 2017; Ramasamy et al., 2017; Wang et al., 2013; Mura et al., 2013; Petkau-Milroy and Brunsveld, 2013). Among the nanocarriers that have been widely studied as potential containers for solubilizing poorly water-soluble drugs and delivering them to their target sites are macrocyclic receptors, such as cyclodextrins (CDs), and aggregates of amphiphilic molecules, such as liposomes (Wu et al., 2016; Qu et al., 2015; Ma and Zhao, 2015; Martínez et al., 2013; Ghosh and Nau, 2012; Li et al., 2014). CDs are a class of biocompatible cyclic oligosaccharides with a truncated cone shape and can be functionalized to encapsulate bioactive substrates in their intrinsically hydrophobic cavities, and liposomes, also biocompatible, are nano- or microscale phospholipid vesicles that can co-encapsulate hydrophilic cargo in their interior aqueous cores and hydrophobic payloads in their lipid-based membranes (Chen and Liu, 2010; Peng et al., 2010; Engel et al., 2018; Mejia-Ariza et al., 2017; Niu et al., 2016). Despite these potentially useful features, few macrocyclic and liposomal systems have been successfully translated from the research laboratory to the clinic, because they suffer from serious drawbacks, such as limited drug-loading efficiency, poor stability, and premature drug release into the blood circulation, and they lack responsiveness to external triggers (Kim et al., 2010). Therefore the development of drug delivery systems that are more effective under physiological conditions is highly imperative.

With a clear understanding of the strengths and weaknesses of CDs and liposomes, researchers have been investigating the integration of CDs and liposomes into supramolecular nanoassemblies. This “drug-in-cyclodextrin-in-liposome” approach attempts to take advantage of the complementarity of the two components for the fabrication of ideal nanocarriers (McCormack and Gregoriadis, 1994; Fernandes Fraceto et al., 2014). This cooperative method has been shown to increase drug solubility and stability, improve control of drug fate *in vivo*, and prevent the rapid release that is often observed when drugs are incorporated into conventional lipid phases (Maestrelli et al., 2006). However, the stability of CD-liposome assemblies is largely dependent on the type and concentration of the CDs (Hatziet al., 2007). Moreover, because CDs and liposomes have no intrinsic therapeutic efficacy, their use decreases the drug-to-carrier mass ratio. However, if CDs and liposomes themselves could cooperatively enhance the therapeutic efficacy of the encapsulated drug, the resultant nanoassemblies might be developed as appealing delivery systems that would combine the advantages of free drugs and nanocarriers.

¹College of Chemistry, State Key Laboratory of Elemento-Organic Chemistry, Nankai University, Tianjin 300071, China

²Collaborative Innovation Center of Chemical Science and Engineering (Tianjin), Tianjin 300072, China

³Lead Contact

*Correspondence: yuliu@nankai.edu.cn

<https://doi.org/10.1016/j.isci.2019.04.029>



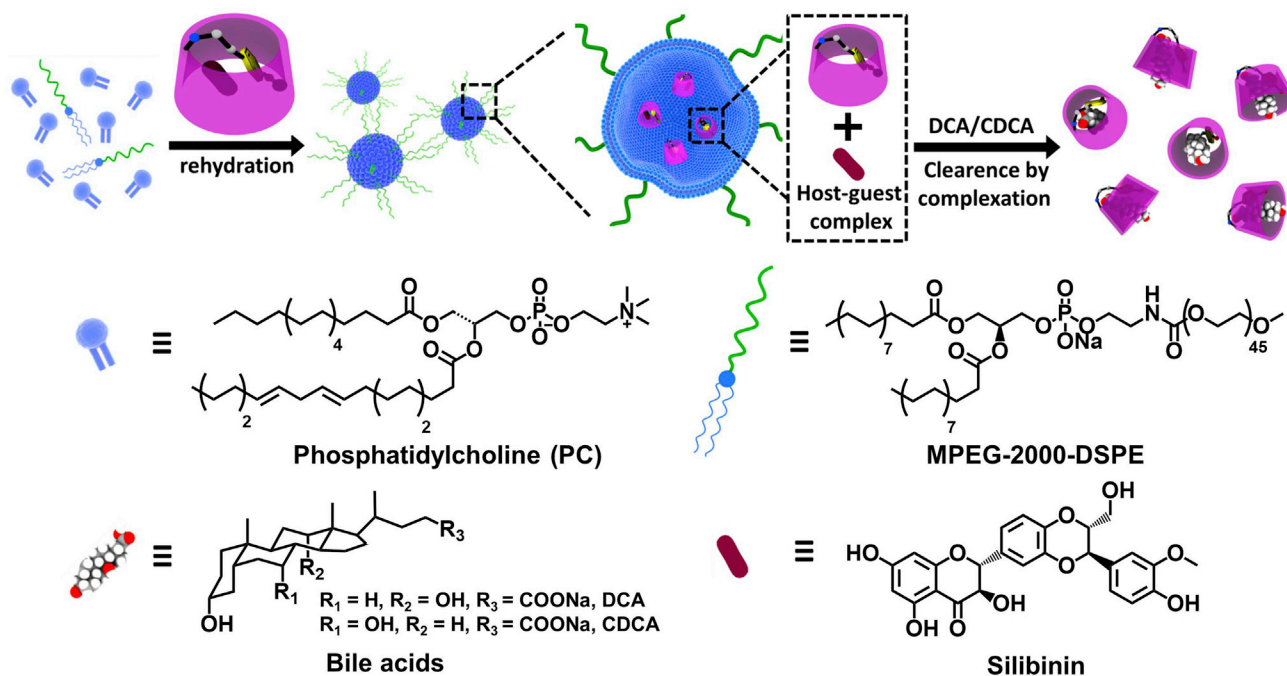


Figure 1. Schematic Illustration of the Drug Displacement and Combinational Treatment Strategy and Structures of a Ternary CD-Liposome Supramolecular Nanoassembly (SLB@1)@PC and Its Components

The nanoassembly was constructed from the SLB@1 complex, the amphiphilic PC, and MPEG-2000-DSPE. After cleavage of the phosphate ester bond of β -CD 1 by alkaline phosphatase in the liver of mice, SLB was released and displaced by cytotoxic BAs (deoxycholic acid [DCA] and chenodeoxycholic acid [CDCA]).

With this goal in mind, we herein describe a novel drug displacement strategy exemplified by the use of ternary CD-liposome supramolecular nanoassemblies containing an active drug molecule to realize both high drug solubilization and efficient clearance of toxic substances. Because the CDs are modified with an enzymatically cleavable functional group, these nanoassemblies may find utility as a multifunctional nanoplatform for enzyme-triggered drug release and targeted tissue accumulation. Specifically, we engineered ternary nanoassemblies consisting of a water-insoluble hepatoprotective drug (silibinin [SLB]), phosphotyramine-modified β -CD (1), and the amphiphilic phosphatidylcholine (PC) for the treatment of acute liver injury (Figure 1). These nanoassemblies demonstrated several inherent advantages. First, solubilization of SLB by 1 resulted in the formation of an SLB@1 host-guest inclusion complex with moderate binding strength. Second, the phosphotyramine group on the primary rim of β -CD 1 made the macrocyclic receptor responsive to the enzyme alkaline phosphatase (ALP), overexpression of which often indicates hepatic dysfunction or injury. Enzymatic cleavage of the phosphate ester group facilitated rapid release of the encapsulated drug at the site of action. More importantly, supramolecular nanoassemblies formed by the interaction of the SLB@1 complex with PC showed targeted accumulation in the liver of mice after intraperitoneal injection. Finally, because 1 strongly bound cytotoxic bile acids (BAs), it could ameliorate exogenous BA-mediated cytotoxicity in a mouse model of acute liver injury by removing excess BAs via host-guest complexation after drug release and displacement. Our results indicate that the use of liposomes in conjunction with a functional CD-based complex is a promising strategy for developing advanced therapies for BA-related hepatic diseases.

RESULTS AND DISCUSSION

Molecular Binding of Drug SLB by β -CDs 1 and 2

Phosphotyramine-modified β -CD 1 was synthesized by a nucleophilic substitution reaction between mono-[6-O-(p-toluenesulfonyl)]- β -CD and phosphotyramine in triethanolamine (Figures S1 and S2) (White and Backer, 1991; Chen et al., 2010). With the phosphotyramine and CD moieties acting as a solubilizer, 1 showed satisfactory solubility in water (>2.0 mM, i.e., 26.7 mg/mL), which is much higher than the solubility of the corresponding tyramine-modified host (2, 0.3 mM, i.e., 3.9 mg/mL). The introduction of the

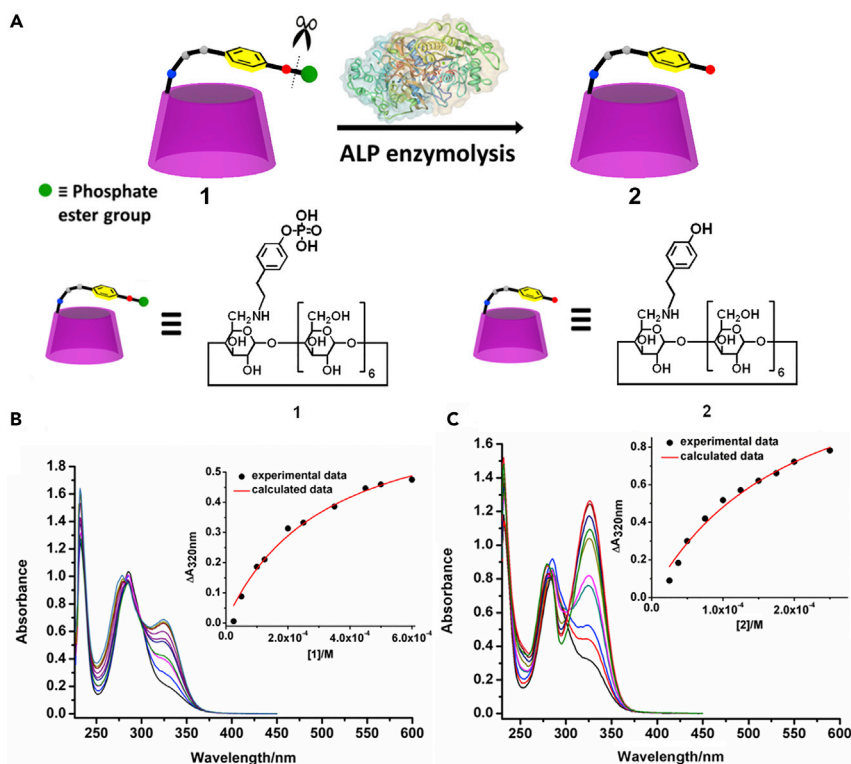


Figure 2. Quantitative Evaluation of the Binding Affinity of SLB for β -CDs 1 and 2

(A) Schematic illustration of the transformation of 1 to 2 by ALP enzymolysis.
 (B) UV-vis spectra of SLB after gradual addition of 1 in water at 25°C. The inset shows nonlinear least-squares analyses of the spectral changes at 320 nm, carried out to calculate the 1:1 stability constants (K_S) of the SLB \subset 1 complexes ([SLB] = 50 μ M, [1] = 0–0.6 mM).
 (C) UV-vis spectra of SLB after gradual addition of 2 in water at 25°C. The inset shows nonlinear least-squares analyses of the spectral changes at 320 nm, carried out to calculate the 1:1 stability constants (K_S) of the SLB \subset 2 complexes ([SLB] = 50 μ M, [2] = 0–0.25 mM).

phosphotyramine group to 1 not only dramatically increased its water solubility but also provided a site that was sensitive to ALP, a biomarker commonly used to evaluate liver function (Figure 2A). The cleavage of the phosphate ester bond in 1 by ALP was confirmed by mass spectrometry; specifically, after incubation of 1 with ALP for 24 h, a new peak, assigned to the corresponding tyramine-pendant product 2, appeared at m/z 1,254.285, and no residual precursor 1 was observed, indicating that it had been completely converted to 2 by the hydrolytic enzyme (Figure S3).

Next, we loaded the drug cargo, SLB, a hepatoprotective biomolecule that is used to treat toxic liver damage. This drug was chosen because its π -conjugated lipophilic skeleton can be well accommodated by the β -CD cavity (Abenavoli et al., 2010; Kellici et al., 2015). The phase solubility curve clearly showed that the solubility of SLB was enhanced by 1; for example, at a concentration of 2.0 mM, 1 was able to solubilize SLB at concentrations as high as 0.08 mM in water (Figure S4). We found that 2 solubilized SLB much better than 1 did under the same experimental condition, indicating the stronger binding affinity of the SLB \subset 2 complexation. Furthermore, the host-guest inclusion of SLB by 1 was quantitatively investigated by means of ultraviolet (UV)-vis spectroscopic titration in water at 25°C (Figure 2B). The UV absorbance of SLB in the range from 300 to 350 nm dramatically increased upon the addition of 1, suggesting conversion of the free drug molecule to the 1-associated species. Moreover, a nonlinear least-squares fit of the absorption change indicated that the stability constant (K_S) of the SLB \subset 1 complex was $3.65 \times 10^3 \text{ M}^{-1}$ (assuming 1:1 stoichiometry). In comparison, the stability constant of the SLB \subset 2 complex under the same experimental conditions was determined to be $5.65 \times 10^3 \text{ M}^{-1}$ (Figure 2C), indicating relatively stronger binding affinity. These moderate binding strengths were expected to facilitate the rapid release of SLB at its site of action via the competitive binding of cytotoxic BAs with β -CD's cavity under physiological conditions.

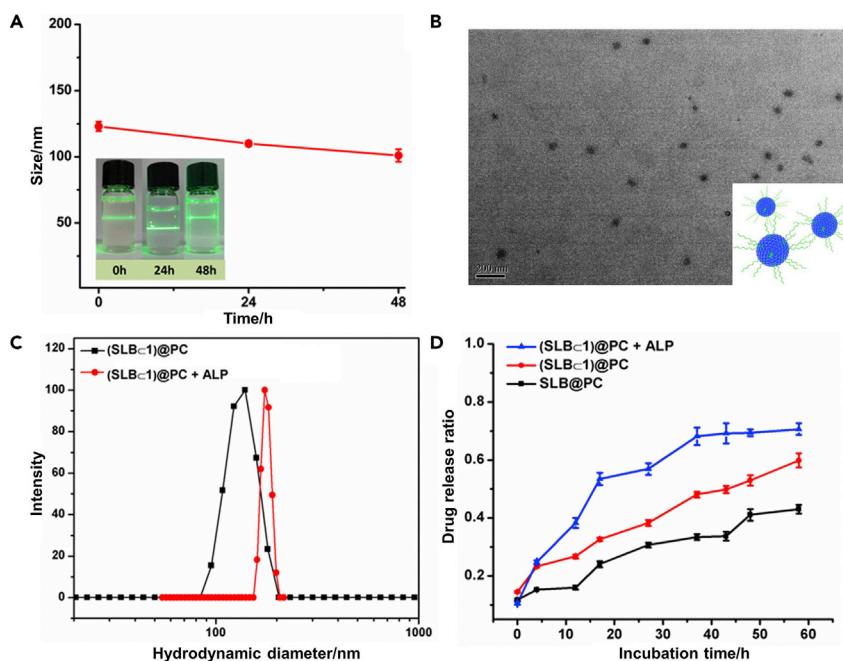


Figure 3. Nanoassembly Construction and Phosphatase-Responsive Drug Release

(A) The stability of the (SLB ≤ 1)@PC nanoassembly in HEPES buffer containing 10% fetal bovine serum was determined by monitoring the size distribution over the course of 48 h. The inset shows the Tyndall effect exhibited by the nanoassemblies over the 48-h period.

(B) TEM image of the nanoassemblies. Scale bar, 200nm.

(C) DLS results for the nanoassemblies before and after treatment with ALP (1 U/mL).

(D) *In vitro* release profiles of SLB from SLB@PC and (SLB ≤ 1)@PC in the presence and absence of ALP (1 U/mL) in HEPES buffer (pH = 7.2, I = 0.01 M) at 37°C ([SLB] = 42 μ M and [1] = 1.0 mM).

Supramolecular Nanoassembly Formation and Phosphatase-Responsive Drug Release

The primary nanoaggregates of amphiphiles were generated by the coassembly of PC and PEGylated 1,2-distearoyl-sn-glycero-3-phosphoethanolamine (MPEG-2000-DSPE) in a 20:1 molar ratio. The resultant liposomes were rehydrated with a solution of the SLB ≤ 1 complex under ultrasonic conditions to obtain the ternary supramolecular (SLB ≤ 1)@PC nanoassemblies (Figure 1). Doping with the PEGylated compound greatly enhanced the water solubility and mechanical stability of the ternary assemblies. More importantly, PEGylation, which is a versatile strategy for nanomedicine formulation, has been shown to protect multi-component nanoparticles from the reticuloendothelial scavenging pathway and to prolong their residence time in the blood circulation (Kolate et al., 2014). The morphology of the (SLB ≤ 1)@PC nanoassemblies was elucidated by means of dynamic light scattering (DLS) and transmission electron microscopy (TEM). The nanoassemblies could be stably dispersed in serum environments and exhibited a clear Tyndall effect, and no size change was observed even after the dispersion was allowed to stand for 48 h (Figure 3A). TEM images showed that the nanoassemblies were uniformly sized (Figure 3B). DLS measurements indicated that their average hydrodynamic diameter was 140 nm and that the diameter was 174 nm in the presence of ALP (Figure 3C). The ALP enzymolysis might seriously disrupt the hydrophilic-hydrophobic balance of the obtained supramolecular nanoparticles, thus leading to the diameter distribution change in the (SLB ≤ 2)@PC nanoassembly (Liu et al., 2018).

More interestingly, we found that the SLB release kinetics depended strongly on the encapsulation conditions (Figure 3D). The encapsulated drug was released relatively slowly from SLB@PC and (SLB ≤ 1)@PC over a period of 58 h. In contrast, the release rate was markedly accelerated when the (SLB ≤ 1)@PC nanoassemblies were treated with ALP, and nearly 80% of the SLB had been released at the end of 58 h; this difference was probably due to the enhanced binding ability of SLB ≤ 2 complexation that could encapsulate more drug molecules out of liposome after enzymolysis (Figure S4B). The serum-resistant stability and enzyme-triggered release behaviors exhibited by the (SLB ≤ 1)@PC nanoassemblies suggested that they

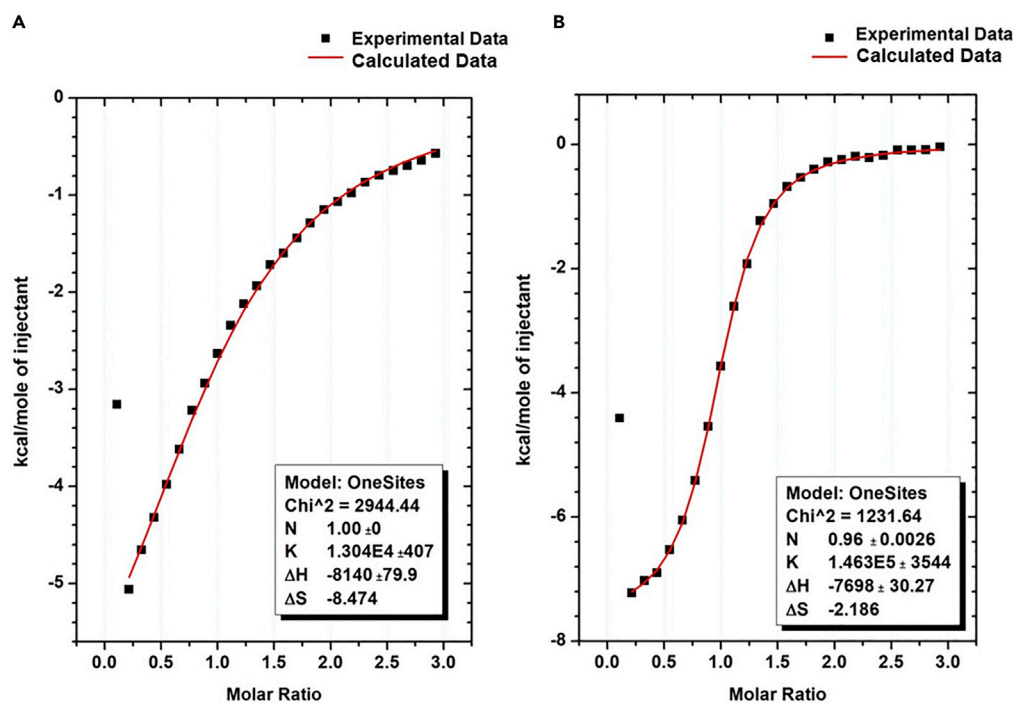


Figure 4. ITC Results for the DCA and CDCA Complexation

(A) ITC isotherms were obtained for the titration of **1** with DCA in 3% DMSO-phosphate buffer solution at 25°C.

(B) ITC isotherms were obtained for the titration of **1** with CDCA in 3% DMSO-phosphate buffer solution at 25°C.

Note that the amount of **1** required to reach binding equilibrium was less for CDCA than for DCA under the same conditions, which indicates that the binding affinity between **1** and CDCA was higher than that between **1** and DCA.

might have targeted delivery capabilities, whereby an active ingredient could be released in the presence of ALP, which is abundantly overexpressed in the injured liver tissue.

Molecular Binding of Cytotoxic BAs by β -CDs **1** and **2**

One of the main clinical manifestations of liver injury is the leakage of cytotoxic BAs, such as deoxycholic acid (DCA) and chenodeoxycholic acid (CDCA), which may cause many adverse outcomes, such as pancreatitis, autoimmune hepatitis, and even hepatocellular carcinoma (Jiao et al., 2015; Muili et al., 2013; Zhang et al., 2015). In this study, we found that in addition to solubilizing SLB, the (SLB \subset 1)@PC nanoassemblies could scavenge BAs after the therapeutic agent SLB had been released. The abilities of **1** and its enzymatic hydrolysate, **2**, to bind frequently encountered cytotoxic BAs (e.g., DCA, and CDCA) were compared in aqueous solution. Taking DCA as examples, typical Job plot revealed an inflexion point at a molar ratio of 1, corresponding to a 1:1 complexation stoichiometry with host **1** at 25°C in D₂O (Figure S5). Rotating frame nuclear Overhauser effect spectroscopy confirmed that the phosphotyramine unit of **1** and tyramine unit of **2** were self-included in the β -CD cavity and were not expelled from the cavity upon complexation with DCA and CDCA (Figures S6 and S7). Moreover, thermodynamic parameters were determined by means of isothermal titration calorimetry (ITC) (Figure 4 and Figures S8A and S8B). The mixed solvent with 3% DMSO-phosphate buffer solution was employed to ensure the complete dissolution of tyramine-modified β -CD. The molecular binding process was enthalpy driven and was accompanied by an unfavorable entropic loss, which was attributed mainly to the combined effect of hydrophobic encapsulation and conformational fixation upon complexation with steroid rings (Table 1). Note that the intermolecular complexation of **1** with CDCA always gave a smaller entropic loss, probably due to excessive desolvation arising from simultaneous inclusion complexation of the bulky phosphotyramine moiety and the polar BA head group in the β -CD cavity. As discerned from the slope and intercept of an enthalpy-entropy compensation plot, it can be concluded that the modified β -CDs **1** and **2** underwent moderate conformational change and extensive desolvation upon binding of BAs (Figure S8C) (Inoue et al., 1993).

Guest	Host	K_S	ΔG°	ΔH°	$T\Delta S^\circ$
DCA	β -CD ^a	2,150 \pm 80	-19.0	-32.0 \pm 0.0	-13.0
	1	13,040 \pm 407	-23.5	-34.1 \pm 0.3	-10.6
	2 ^a	15,650 \pm 650	-23.9	-46.6 \pm 1.7	-22.7
CDCA	β -CD	60,700 \pm 4,630	-27.3	-30.7 \pm 0.6	-3.4
	1	146,300 \pm 3,544	-29.5	-32.2 \pm 0.1	-2.3
	2	182,500 \pm 3,420	-30.0	-39.9 \pm 0.1	-9.9

Table 1. Evaluation of Molecular Binding Behaviors by ITC Method

Complex stability constants (K_S/M^{-1}), standard free energy ($\Delta G^\circ/kJ\cdot mol^{-1}$), enthalpy ($\Delta H^\circ/kJ\cdot mol^{-1}$), and entropy changes ($T\Delta S^\circ/kJ\cdot mol^{-1}$) for 1:1 inclusion complexation of BAs by host CDs in 3% DMSO-phosphate buffer solution (pH 7.2, $I = 0.1$ M) at 25.00°C.

^aRef (Zhang et al., 2017).

Moreover, compared with the K_S values for binding of BAs to native β -CD, the K_S values for binding of BAs to **1** and **2** were dramatically higher, which we attributed mainly to the favorable electrostatic attraction between the protonated amino group of the hosts and the carboxylic tail of the guests. It is also noteworthy that the K_S values of the CDCA \leq **1** and CDCA \leq **2** complexes reached $10^5 M^{-1}$ in aqueous solution, probably because the size of CDCA allowed it to fully occupy the β -CD cavity. Taken together, the ITC results demonstrate that the binding of BAs was tighter after enzymatic hydrolysis by ALP and that thermodynamically stable complexation would ensure that SLB would be readily displaced by cytotoxic BAs and then the β -CDs could clear cytotoxic BAs in a drug displacement process, both *in vitro* and *in vivo*, as will be described below.

In Vitro Reversal of BA-Induced Cytotoxicity by β -CDs **1** and **2**

Two types of cell lines that are ultrasensitive to BA-induced cytotoxicity (HT-29 and HCT-116) were used to evaluate the ability of **1** to reverse the cytotoxic effects of DCA at a cellular level (Figure 5A). In preliminary experiments, incubation of both cell lines with free **1** for 24 and 48 h revealed that cell viability remained at nearly 100% throughout the incubation period, indicating that this phosphotyramine-modified host was nontoxic and highly biocompatible (Figure S9). In the subsequent PrestoBlue assays, we incubated the cells with DCA and a sufficient amount of **1** to ensure maximum conversion to inclusion complexes and to achieve optimal reversal of DCA toxicity in the cellular environment.

We found that the dose-dependent cytotoxicity of DCA was greatly suppressed by the presence of **1** and that the effect was greater at 48 h than at 24 h (Figures 5B–5E). For example, when the DCA concentration was 300 μ M, the relative cellular viability of the HCT-116 cells after incubation for 48 h was significantly higher in the presence of **1** (70%) than in its absence (30%). Given the noncovalent molecular binding characteristics, more free cytotoxic BAs can exist in the exchange equilibrium of host-guest complexation, which may induce more serious cytotoxicity in the cellular environment. Therefore we can infer that phosphotyramine-modified β -CD **1** possessed potent and sustained activity against the cytotoxicity induced by BA accumulation, and we attributed this activity to the effects of host-guest complexation of the BAs. Comparison of the abilities of **1** and **2** to reverse the effects of DCA revealed no obvious difference in the efficiency of viability recovery (Figures 5F and S10). That is, host **2** maintained its reversal capacity to cytotoxic BAs after enzymolysis.

In Vivo Evaluation of the Drug Displacement Strategy for Treatment of Acute Liver Injury with Ternary CD-Liposome Nanoassemblies

First, we used confocal laser scanning microscopy to confirm cellular uptake of the CD-liposome nanoassemblies. For this purpose, host **1** encapsulated an adamantane (ADA)-modified cyanine dye (Cy5) because the binding affinity between β -CD **1** and ADA is much higher than that between **1** and SLB (Sun et al., 2015). After incubation of NIH 3T3 mouse embryonic fibroblasts with the (ADA-Cy5 \leq **1**)@PC nanoassemblies for 6 h at 37°C, the cells showed the bright red fluorescence of Cy5 (Figure S11). Having validated cellular uptake, we next investigated whether the nanoassemblies could selectively accumulate in mouse liver. We found that 60 min after intravenous injection of the (ADA-Cy5 \leq **1**)@PC nanoassemblies in the right hind

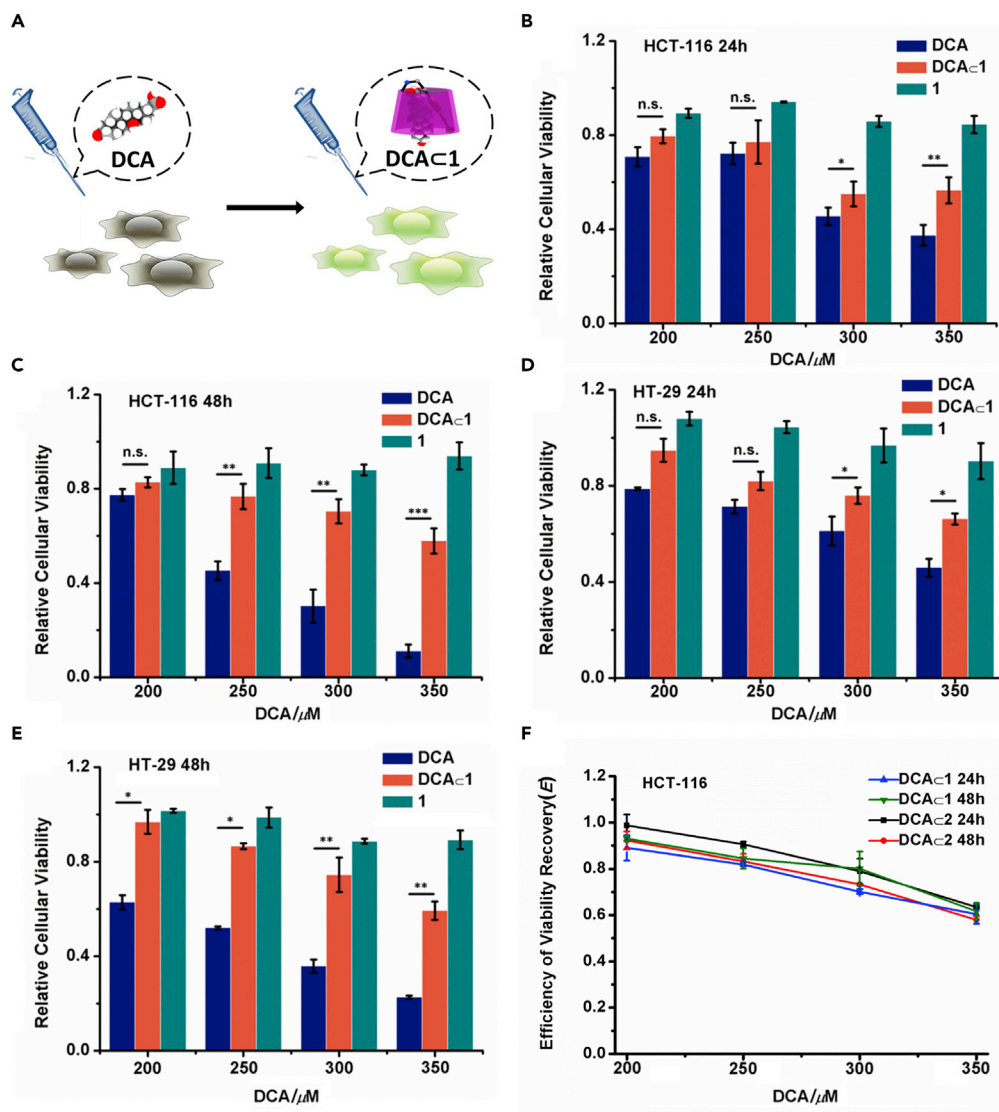


Figure 5. In Vitro Evaluation of the Ability of β -CD 1 to Clear DCA

(A) Schematic illustration of the inhibitory effect of 1 on DCA-induced cytotoxicity.

(B) Relative viabilities of HCT-116 cells 24 h after addition of DCA, 1, or DCA \subset 1.

(C) Relative viabilities of HCT-116 cells 48 h after addition of DCA, 1, or DCA \subset 1.

(D) Relative viabilities of HT-29 cells 24 hr after addition of DCA, 1, or DCA \subset 1.

(E) Relative viabilities of HT-29 cells 48 h after addition of DCA, 1, or DCA \subset 1.

(F) Efficiency of viability recovery (E) of HT-116 cells after 24- and 48-hr incubation with DCA \subset 1 and DCA \subset 2 inclusion complexes. The E values for host 2 were obtained from Zhang et al. (2017).

Statistically significant differences are indicated with asterisks (***p < 0.001, **p < 0.01, *p < 0.05, and n.s., not significant). Binding constant calculations indicated that more than 90% of the DCA was converted to the DCA \subset 1 inclusion complex in these experiments.

leg of mice, high fluorescence emission was observed in the liver area (Figure 6B), suggesting that (ADA-Cy5 \subset 1)@PC had accumulated there.

Next, we investigated the effects of treatment with the (SLB \subset 1)@PC nanoassemblies in mice with acute liver injury induced by carbon tetrachloride (CCl₄, Figure 6A) (Hermenean et al., 2014). To assess the recovery of liver function, we monitored the levels of ALP, alanine aminotransferase (ALT), and total bile acids (TBA). As shown in Figures 6C–6E, we found that in mice that had been intraperitoneally injected with

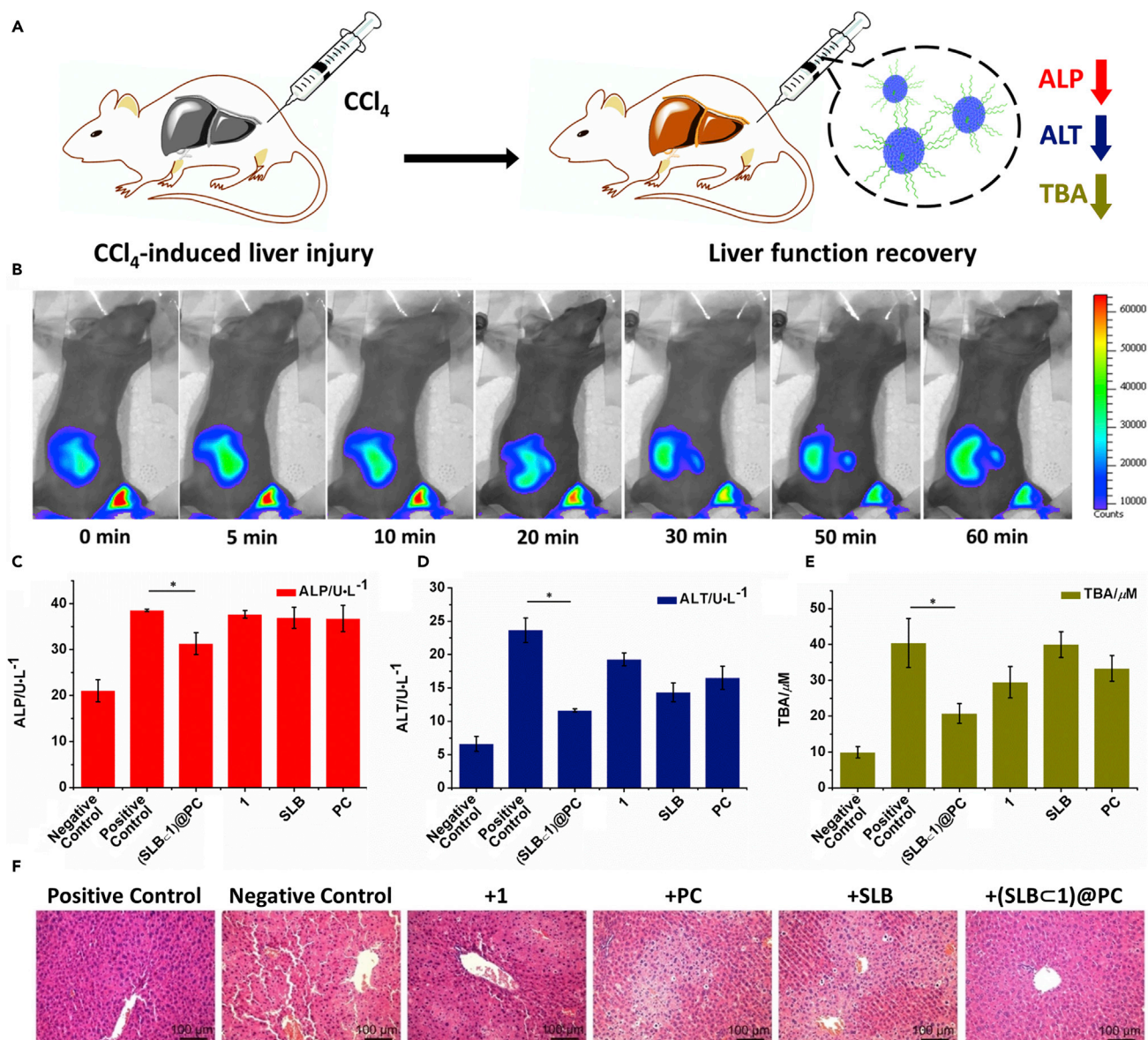


Figure 6. In Vivo Evaluation of the Therapeutic Effects of (SLB \subset 1)@PC Nanoassemblies in A Mouse Model of Acute Liver Injury

(A) Schematic illustration of experiments with (SLB \subset 1)@PC nanoassemblies in mice.

(B) *In vivo* fluorescence microscopy images of mice from 0 to 60 min after intravenous injection of (Ada-Cy5 \subset 1)@PC nanoassemblies via the right hind leg.

(C) Variation of blood ALP levels 20 h after injection of CCl₄ and subsequent treatment with (SLB \subset 1)@PC or one of the individual components.

(D) Variation of blood ALT levels 20 h after injection of CCl₄ and subsequent treatment with (SLB \subset 1)@PC or one of the individual components.

(E) Variation of blood TBA levels 20 h after injection of CCl₄ and subsequent treatment with (SLB \subset 1)@PC or one of the individual components (statistically significant differences are indicated with asterisks, *p < 0.05).

(F) Histological observations of H&E-stained liver sections after treatment with (SLB \subset 1)@PC or one of its components.

CCl₄, the serum levels of ALP (38.6 U L⁻¹) and ALT (23.7 U L⁻¹) were markedly higher than in control mice, and that the TBA concentration was also higher (40.4 μM), indicating liver failure in the treated mice. There was no obvious change in ALP level after treatment with SLB, 1, or PC alone; however, in mice that were treated with the (SLB \subset 1)@PC nanoassemblies, the ALP level was only 31.3 U L⁻¹. In contrast, the blood ALT levels in mice treated with the individual components of the nanoassemblies were lower than the levels in the positive controls, particularly for the mice treated with the hepatoprotective drug SLB. However, as expected, the lowest ALT level was observed in mice treated with the (SLB \subset 1)@PC nanoassemblies

(11.6 U L^{-1}), which is attributed to the cooperative effects of the multiple components. This result was also consistent with the conclusion that PC as the major membrane phospholipid could stabilize cell membrane and enhance cell membrane integrity (Chamulitrat et al., 2012). Interestingly, the TBA concentrations in the mice treated with **1** alone or with liposome alone were much lower than the concentration in the mice treated with SLB alone. This result seems reasonable given that both β -CDs and liposomes can be expected to incorporate the steroid skeleton of BAs into their hydrophobic microenvironment. More importantly, a large proportion of the BAs was cleared from the blood in the mice treated with the (SLB \subset **1**)@PC nanoassemblies ([BA] = $20.7 \text{ }\mu\text{M}$), again corroborating the efficacy of our drug displacement strategy for clearing toxic BAs *in vivo*. Furthermore, histological observation showed that the integrity of hepatic tissues was seriously compromised by CCl_4 injection, but it was clearly restored after treatment with the (SLB \subset **1**)@PC nanoassemblies (Figure 6F).

Overall, the *in vivo* animal experiments demonstrate that liver injury could be largely reversed by the cooperative protective effect of the (SLB \subset **1**)@PC nanoassemblies. More significantly, owing to the strong non-covalent interaction between the BAs and the CD units after displacement of drug cargo, the cytotoxic BAs could be efficiently removed from the mouse blood via host-guest inclusion complexation, restoring the TBA concentration to a normal level.

Conclusion

In summary, we have described a drug displacement strategy for solubilizing a water-insoluble drug and rapidly removing cytotoxic BAs with a single therapeutic agent, a ternary CD-liposome supramolecular nanoassembly. We demonstrated that the hepatoprotective drug SLB could be encapsulated in the cavity of phosphotyramine-modified β -CD **1** and that ternary (SLB \subset **1**)@PC nanoassemblies could subsequently be obtained by rehydration of the SLB \subset **1** complex with PC. The uniformly sized (SLB \subset **1**)@PC nanoassemblies accumulated selectively in the liver of mice. Interestingly, enzymolysis of the phosphate ester bond by ALP accelerated the release of SLB from the core of the liposomes. ITC experiments and cell viability tests revealed that the cytotoxicity of BAs released from liver tissue injured by injection of CCl_4 could be largely reversed by supramolecular complexation of the BAs within the β -CD after release of the encapsulated SLB, due to the much higher binding affinity of the β -CD's cavity with the cytotoxic BAs. Moreover, CCl_4 -induced intoxication could be attenuated by injection of the (SLB \subset **1**)@PC nanoassemblies. Specifically, we found that treatment with the nanoassemblies resulted in decreased blood levels in ALP and ALT, and that the leaked endogenous BAs arising from liver injury could be rapidly removed from the bodies of the mice by the cooperative action of the β -CDs and PC. The multifunctional nanoassemblies described herein are superior to conventional nanocarriers because both the β -CDs and the PC actively contributed to the therapeutic effect. In a mouse model, the nanoassemblies solubilized an active drug, released it in an enzyme-responsive fashion in the target tissue, and acted as "detergent" to clear toxic BAs. This drug displacement strategy definitely shows promise for the construction of new multifunctional drug delivery systems.

METHODS

All methods can be found in the accompanying [Transparent Methods supplemental file](#).

Limitations of Study

In this study, a drug displacement strategy was presented and exemplified by an ALP-responsive (drug \subset CD)@liposome ternary assembly. The obtained particulate assembly can specifically accumulate in the liver of mice and then clear the cytotoxic BAs via the competitive binding with β -CD's cavity. However, more preclinical models are necessary to validate these findings. More appropriate stimuli-responsive sites with distinct molecular binding abilities toward some bioactive substrates can be attempted to integrate with the above-mentioned nanoassembly to further enhance the biological performance.

SUPPLEMENTAL INFORMATION

Supplemental Information can be found online at <https://doi.org/10.1016/j.isci.2019.04.029>.

ACKNOWLEDGMENTS

This work was financially funded by the National Natural Science Foundation of China (grants 21432004, 21871154, 21772099, and 21861132001); dedicated to 100th anniversary of Nankai University.

AUTHOR CONTRIBUTIONS

Y.-M.Z. and Y.L. conceived and directed the study. X.X. synthesized CD derivatives and their complexes. Q.Y. and X.X. conducted the cellular and animal experiments. X.X. and H.-J.Y. calculated the thermodynamic parameters. Y.-M.Z. wrote the main manuscript. X.X. and Y.-M.Z. prepared the figures. Y.L. supervised the work and edited the manuscript. All authors analyzed and discussed the results. All authors reviewed the manuscript.

DECLARATION OF INTERESTS

The authors declare that they have no competing interests.

Received: February 2, 2019

Revised: March 26, 2019

Accepted: April 22, 2019

Published: May 31, 2019

REFERENCES

- Abenavoli, L., Capasso, R., Milic, N., and Capasso, F. (2010). Milk thistle in liver diseases: past, present, future. *Phytother. Res.* **24**, 1423–1432.
- Chamulitrat, W., Zhang, W., Xu, W., Pathil, A., Setchell, K., and Stremmel, W. (2012). Hepatoprotectant ursodeoxycholy lysophosphatidylethanolamide increasing phosphatidylcholine levels as a potential therapy of acute liver injury. *Front. Physiol.* **3**, 24.
- Chen, Y., and Liu, Y. (2010). Cyclodextrin-based bioactive nanosupramolecules. *Chem. Soc. Rev.* **39**, 495–505.
- Chen, Y., Li, F., Liu, B.-W., Jiang, B.-P., Zhang, H.-Y., Wang, L.-H., and Liu, Y. (2010). Thermodynamic origin of selective binding of β -cyclodextrin derivatives with chiral chromophoric substituents toward steroids. *J. Phys. Chem. B* **114**, 16147–16155.
- Cheng, H.-B., Zhang, Y.-M., Liu, Y., and Yoon, J. (2019). Turn-on supramolecular host–guest nanosystems as theranostics for cancer. *Chem* **5**, 553–574.
- Engel, S., Möller, N., and Ravoo, B.J. (2018). Stimulus-responsive assembly of nanoparticles using host–guest interactions of cyclodextrins. *Chem. Eur. J.* **24**, 4741–4748.
- Fernandes Fraceto, L., Grillo, R., and Sobarzo-Sanchez, E. (2014). Cyclodextrin inclusion complexes loaded in particles as drug carrier systems. *Curr. Top. Med. Chem.* **14**, 518–525.
- Ghosh, I., and Nau, W.M. (2012). The strategic use of supramolecular pKa shifts to enhance the bioavailability of drugs. *Adv. Drug Deliv. Rev.* **64**, 764–783.
- Hatzl, P., Mourtas, S., Klepetsanis, P.G., and Antimisariaris, S.G. (2007). Integrity of liposomes in presence of cyclodextrins: effect of liposome type and lipid composition. *Int. J. Pharm.* **333**, 167–176.
- Hermenean, A., Ardelean, A., Stan, M., Hadaruga, N., Mihali, C.-V., Costache, M., and Dinischiotu, A. (2014). Antioxidant and hepatoprotective effects of naringenin and its β -cyclodextrin formulation in mice intoxicated with carbon tetrachloride: a comparative study. *J. Med. Food* **17**, 670–677.
- Inoue, Y., Liu, Y., Tong, L.-H., Shen, B.-J., and Jin, D.-S. (1993). Calorimetric titration of inclusion complexation with modified β -cyclodextrins. Enthalpy-entropy compensation in host–guest complexation: from ionophore to cyclodextrin and cyclophane. *J. Am. Chem. Soc.* **115**, 10637–10644.
- Jiao, L., Gan-Schreier, H., Tuma-Kellner, S., Stremmel, W., and Chamulitrat, W. (2015). Sensitization to autoimmune hepatitis in group VIA calcium-independent phospholipase A2-null mice led to duodenal villous atrophy with apoptosis, goblet cell hyperplasia and leaked bile acids. *Biochim. Biophys. Acta* **1852**, 1646–1657.
- Kellici, T.F., Ntountaniotis, D., Leonis, G., Chatziathanasiadou, M., Chatzikonstantinou, A.V., Becker-Baldus, J., Glaubitz, C., Tzakos, A.G., Viras, K., Chatzigeorgiou, P., et al. (2015). Investigation of the interactions of silibinin with 2-hydroxypropyl- β -cyclodextrin through biophysical techniques and computational methods. *Mol. Pharmaceutics* **12**, 954–965.
- Kim, S., Shi, Y., Kim, J.Y., Park, K., and Cheng, J.-X. (2010). Overcoming the barriers in micellar drug delivery: loading efficiency, in vivo stability, and micelle–cell interaction. *Expert Opin. Drug Deliv.* **7**, 49–62.
- Kitagishi, H., and Minegishi, S. (2017). Iron(II) porphyrin–cyclodextrin supramolecular complex as a carbon monoxide-depleting agent in living organisms. *Chem. Pharm. Bull.* **65**, 336–340.
- Kolate, A., Baradia, D., Patil, S., Vhora, I., Kore, G., and Misra, A. (2014). PEG – a versatile conjugating ligand for drugs and drug delivery systems. *J. Control Release* **192**, 67–81.
- Li, Y., Xiao, K., Zhu, W., Deng, W., and Lam, K.S. (2014). Stimuli-responsive cross-linked micelles for on-demand drug delivery against cancers. *Adv. Drug Deliv. Rev.* **66**, 58–73.
- Liu, J.-H., Wu, X., Zhang, Y.-M., and Liu, Y. (2018). Photocleavable supramolecular polysaccharide nanoparticles for targeted drug release in cancer cells. *Asian J. Org. Chem.* **7**, 2444–2447.
- Ma, X., and Zhao, Y. (2015). Biomedical applications of supramolecular systems based on host–guest interactions. *Chem. Rev.* **115**, 7794–7839.
- Maestrelli, F., González-Rodríguez, M.L., Rabasco, A.M., and Mura, P. (2006). Effect of preparation technique on the properties of liposomes encapsulating ketoprofen–cyclodextrin complexes aimed for transdermal delivery. *Int. J. Pharm.* **312**, 53–60.
- Martínez, Á., Ortiz Mellet, C., and García Fernández, J.M. (2013). Cyclodextrin-based multivalent glycoconjugates: covalent and supramolecular conjugates to assess carbohydrate–protein interactions. *Chem. Soc. Rev.* **42**, 4746–4773.
- McCormack, B., and Gregoriadis, G. (1994). Drugs-in-cyclodextrins-in liposomes: a novel concept in drug delivery. *Int. J. Pharm.* **112**, 249–258.
- Mejia-Ariza, R., Graña-Suárez, L., Verboom, W., and Huskens, J. (2017). Cyclodextrin-based supramolecular nanoparticles for biomedical applications. *J. Mater. Chem. B* **5**, 36–52.
- Muili, K.A., Wang, D., Orabi, A.I., Sarwar, S., Luo, Y., Javed, T.A., Eisses, J.F., Mahmood, S.M., Jin, S., Singh, V.P., et al. (2013). Bile acids induce pancreatic acinar cell injury and pancreatitis by activating calcineurin. *J. Biol. Chem.* **288**, 570–580.
- Mura, S., Nicolas, J., and Couvreur, P. (2013). Stimuli-responsive nanocarriers for drug delivery. *Nat. Mater.* **12**, 991–1003.
- Niu, Z., Conejos-Sánchez, I., Griffin, B.T., O’Driscoll, C.M., and Alonso, M.J. (2016). Lipid-based nanocarriers for oral peptide delivery. *Adv. Drug Deliv. Rev.* **106**, 337–354.
- Peng, L., Liu, S., Feng, A., and Yuan, J. (2010). Polymeric nanocarriers based on cyclodextrins for drug delivery: host–guest interaction as stimuli responsive linker. *Mol. Pharmaceutics* **14**, 2475–2486.
- Petkau-Milroy, K., and Brunsveld, L. (2013). Supramolecular chemical biology; bioactive

synthetic self-assemblies. *Org. Biomol. Chem.* **11**, 219–232.

Pugliese, E., Coentro, J.Q., and Zeugolis, J.Q. (2018). Advancements and challenges in multidomain multicargo delivery vehicles. *Adv. Mater.* **30**, 1704324.

Qu, D.-H., Wang, Q.-C., Zhang, Q.-W., Ma, X., and Tian, H. (2015). Photoresponsive host–guest functional systems. *Chem. Rev.* **115**, 7543–7588.

Ramasamy, T., Ruttala, H.B., Gupta, B., Poudel, B.K., Choi, H.G., Yong, C.S., and Kim, J.O. (2017). Smart chemistry-based nanosized drug delivery systems for systemic applications: a comprehensive review. *J. Control Release* **258**, 226–253.

Sun, M., Zhang, H.-Y., Zhao, Q., Hu, X.-Y., Wang, L.-H., Liu, B.-W., and Liu, Y. (2015). A supramolecular brush polymer via the self-assembly of bridged tris(β -cyclodextrin) with a porphyrin derivative and its magnetic resonance imaging. *J. Mater. Chem. B* **3**, 8170–8179.

Wang, L., Li, L.-l., Fan, Y.-s., and Wang, H. (2013). Host–guest supramolecular nanosystems for cancer diagnostics and therapeutics. *Adv. Mater.* **25**, 3888–3898.

White, M.F., and Backer, J.M. (1991). Preparation and use of anti-phosphotyrosine antibodies to study structure and function of insulin receptors. *Methods Enzymol.* **201**, 65–79.

Wu, X., Gao, L., Hu, X.-Y., and Wang, L. (2016). Supramolecular drug delivery systems based on water-soluble pillar[n]arenes. *Chem. Rec.* **16**, 1216–1227.

Zhang, W., Zhou, L., Yin, P., Wang, J., Lu, X., Wang, X., Chen, J., Lin, X., and Xu, G. (2015). A weighted relative difference accumulation algorithm for dynamic metabolomics data: long-term elevated bile acids are risk factors for hepatocellular carcinoma. *Sci. Rep.* **5**, 8984.

Zhang, Y.-M., Xu, X., Yu, Q., Liu, Y.-H., Zhang, H.-Y., Chen, L.-X., and Liu, Y. (2017). Reversing the cytotoxicity of bile acids by supramolecular encapsulation. *J. Med. Chem.* **60**, 3266–3274.

ISCI, Volume 15

Supplemental Information

**Drug Displacement Strategy for Treatment of Acute
Liver Injury with Cyclodextrin-Liposome Nanoassembly
Ying-Ming Zhang, Xun Xu, Qilin Yu, Hua-Jiang Yu, and Yu Liu**

Supplemental data items

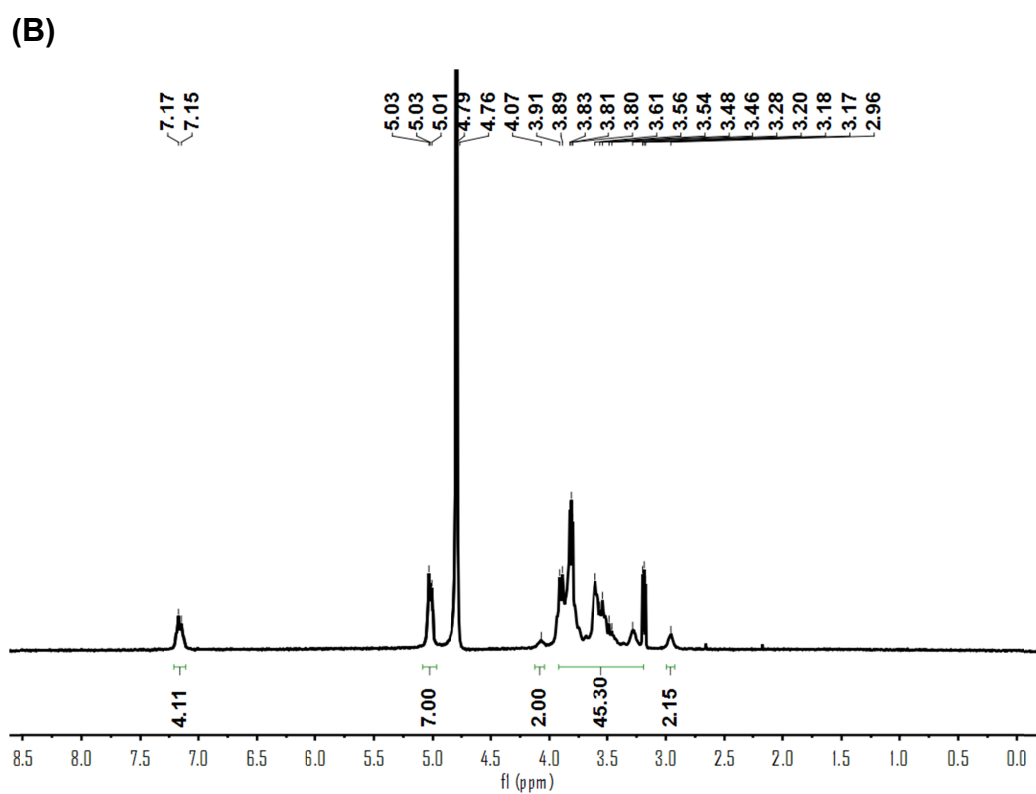
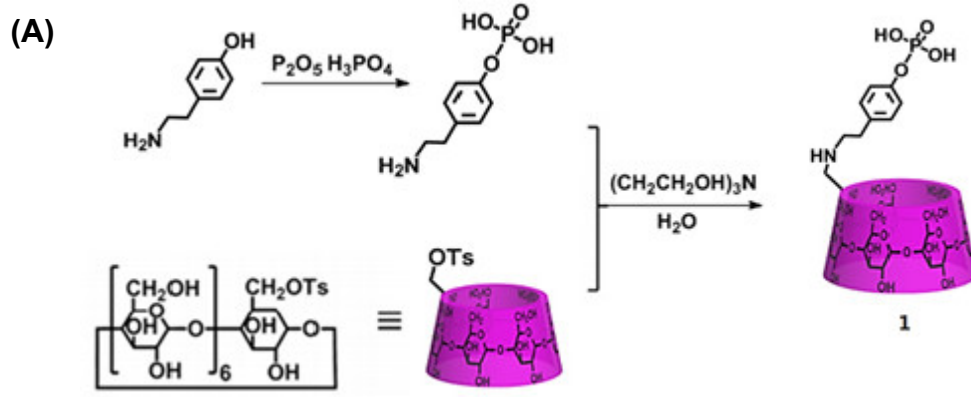


Figure S1. Compound Characterization. (A) Synthetic route of host 1 and (B) 1H NMR spectrum of 1 (400 MHz, D_2O , 25 °C), related to Figure 1.

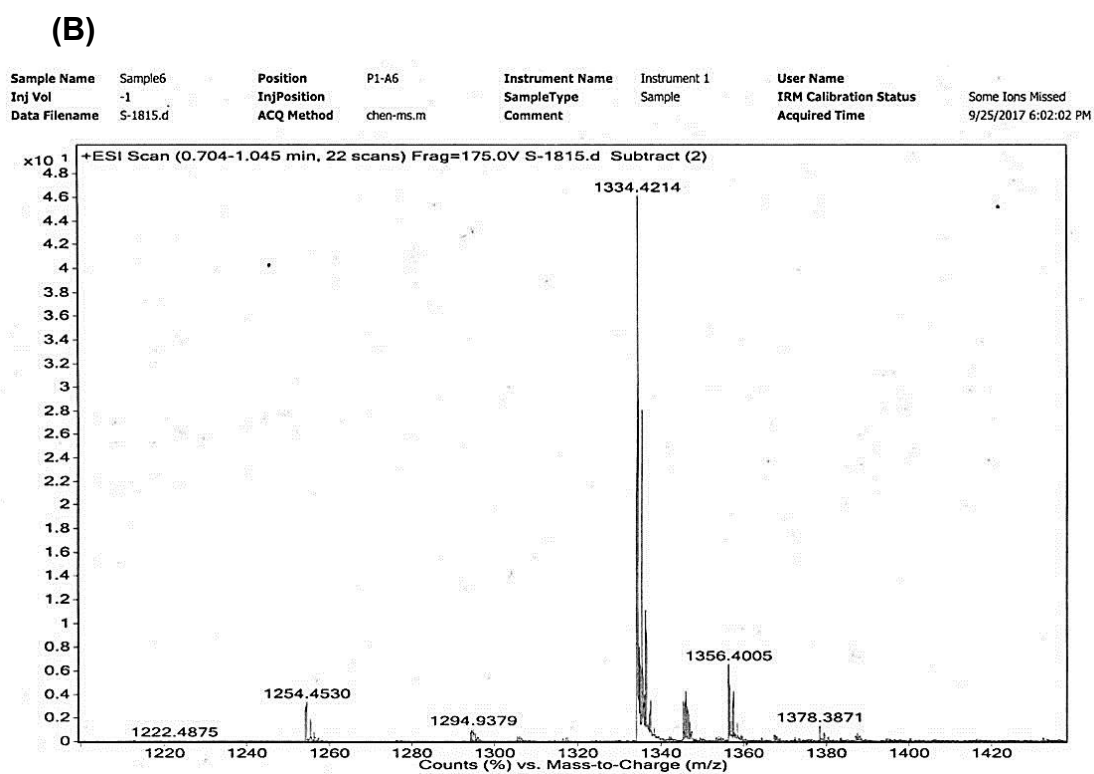
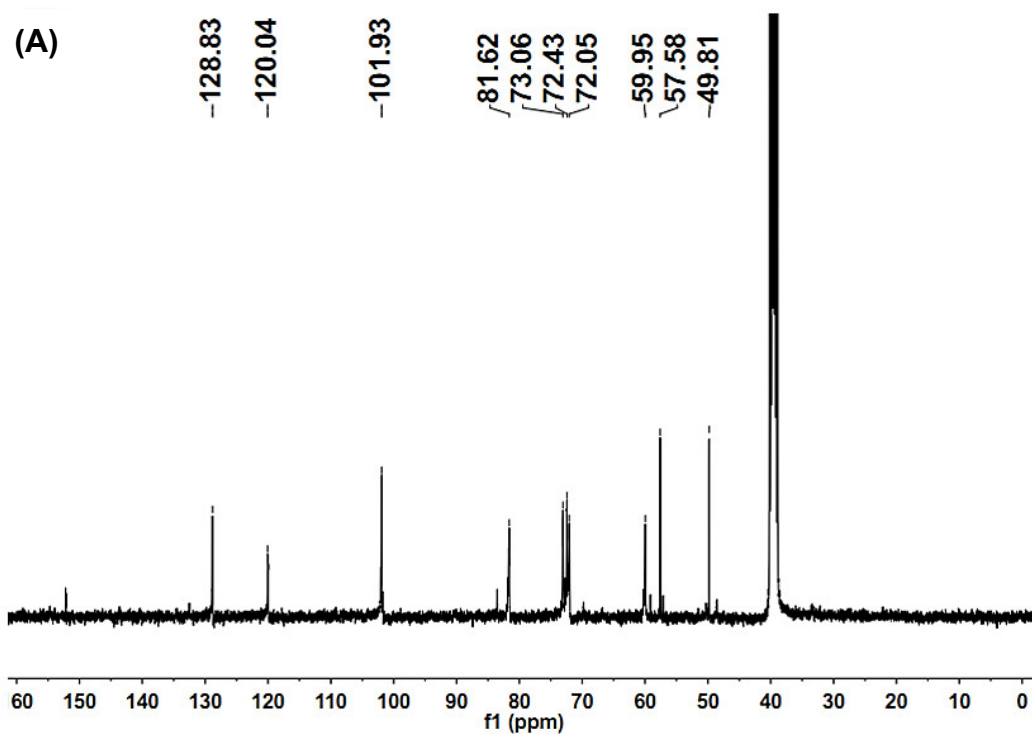


Figure S2. Compound Characterization. (A) ^{13}C NMR spectrum of 1 (101 MHz, DMSO- d_6 , 25 °C) and (B) ESI mass spectrum of 1, related to Figure 1.

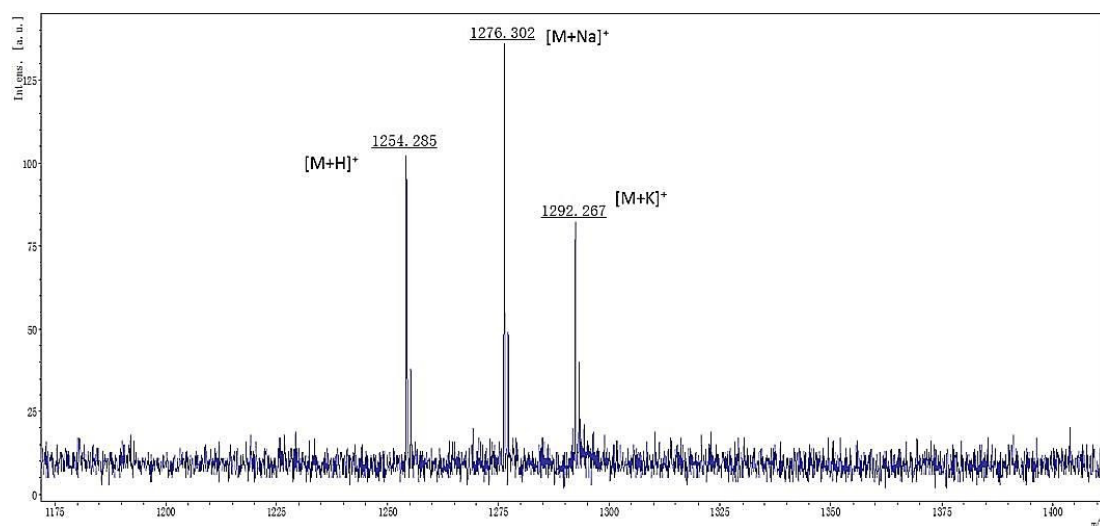


Figure S3. MALDI-TOF spectrum of generated by treatment of 1 with ALP (1 U/mL) in PBS (pH 7.4) after 24 h, related to Figure 2.

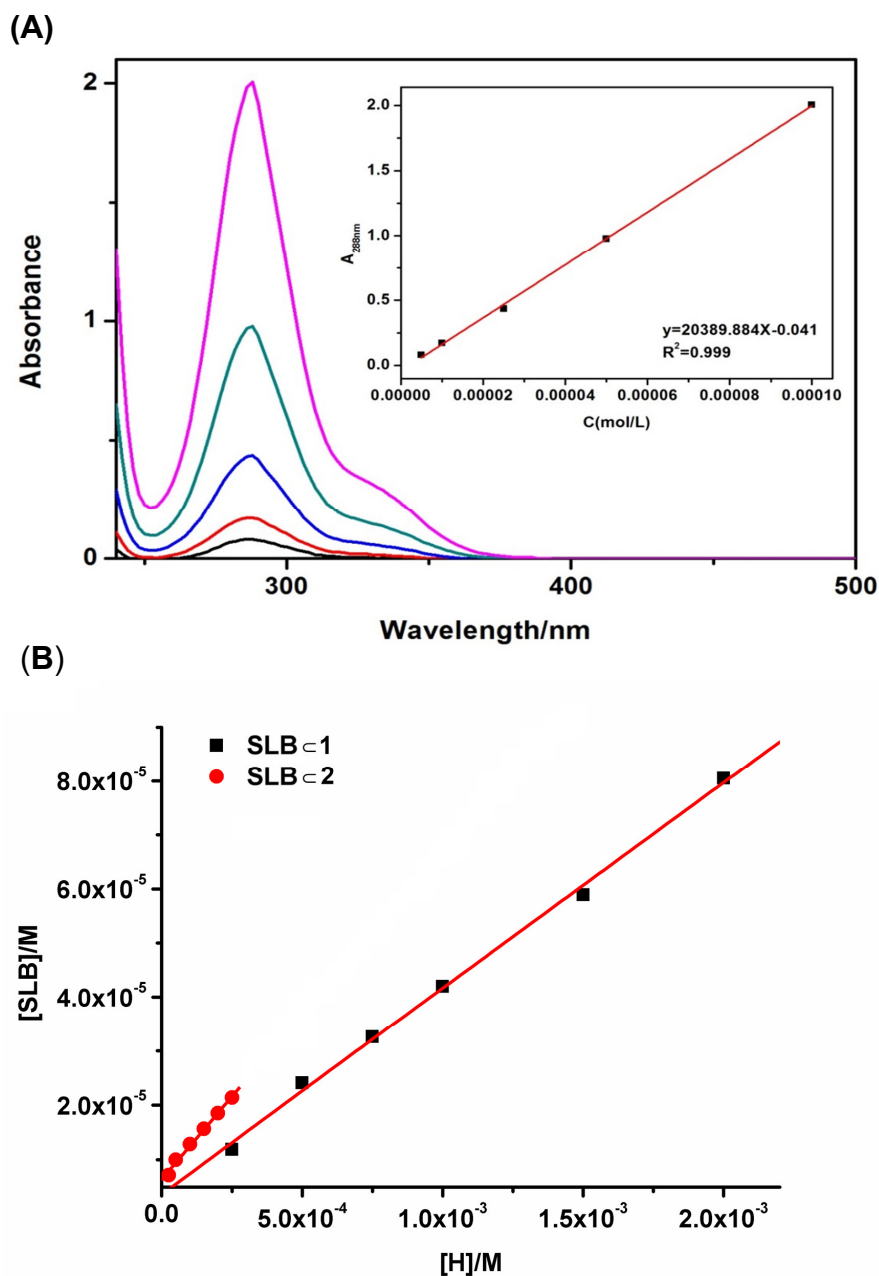


Figure S4. Phase-solubility curves of SLB with hosts 1 and 2. (A) UV/Vis absorption spectra of SLB at 5, 10, 25, 50 and 100 μM in DMSO; (B) phase solubility curve of SLB_c1 and SLB_c2 complexation. Note that no data could be obtained above 0.25 mM of host 2 because of its limited water solubility, related to Figure 3.

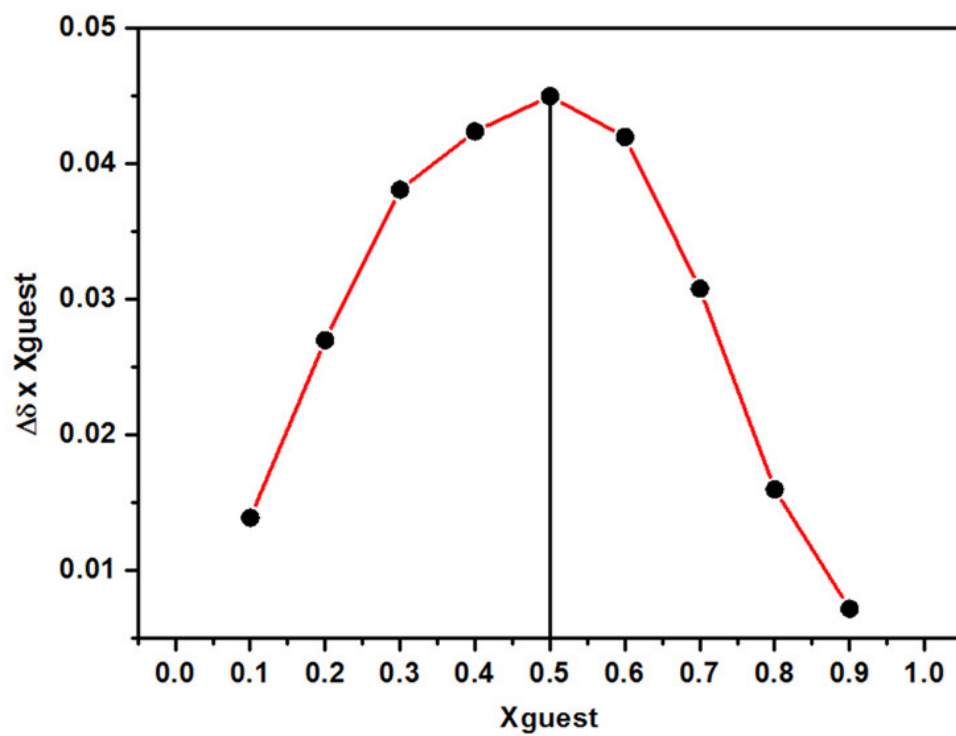


Figure S5. Job plot of DCA \subset 1 complexation ($[1] + [\text{DCA}] = 0.5 \text{ mM}$), related to **Figure 4**.

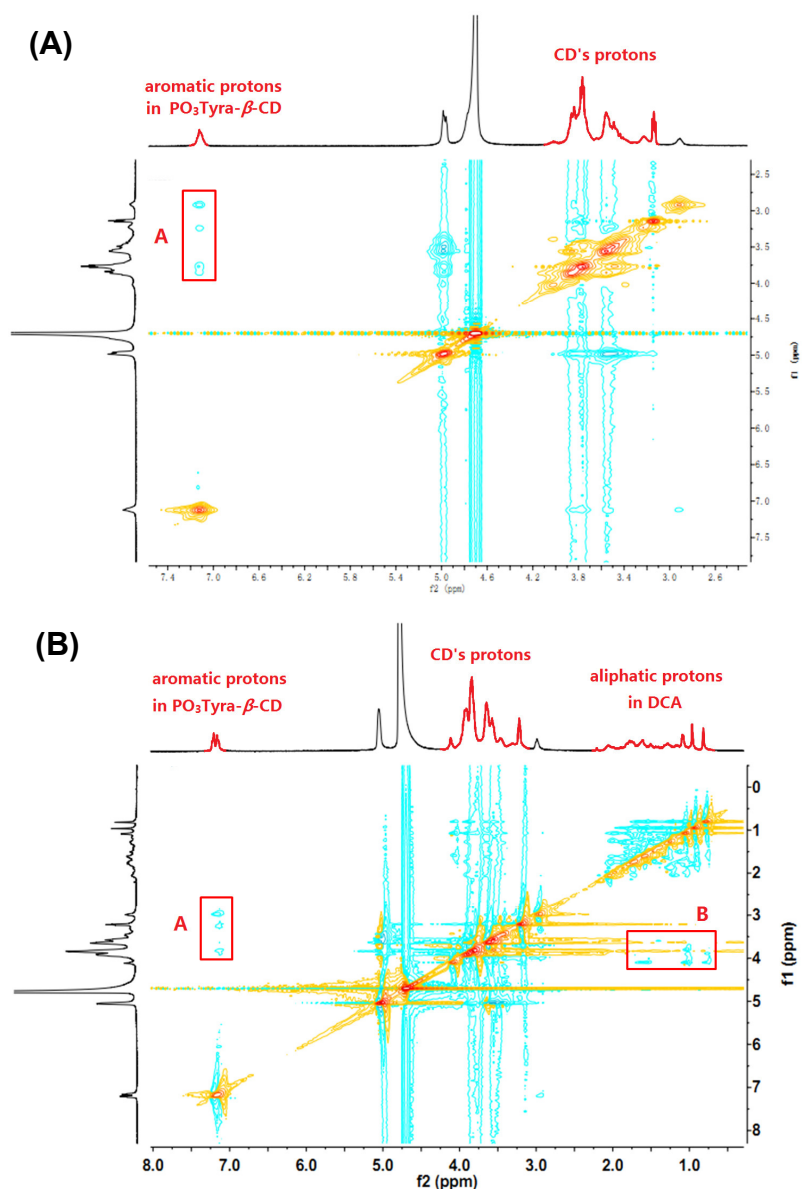


Figure S6. Conformation analyses of inclusion complexation. (A) ¹H ROESY spectrum of free 1 and (B) DCA⊂1 complex after a mixing time of 0.30 s (300 MHz, D₂O, 25 °C). The encircled peaks A were assigned to the NOE correlations between phosphotyramine substituent and β-CD's cavity and encircled peaks B were assigned to the NOE correlations between the steroid skeleton of DCA and β-CD's cavity, related to Table 1.

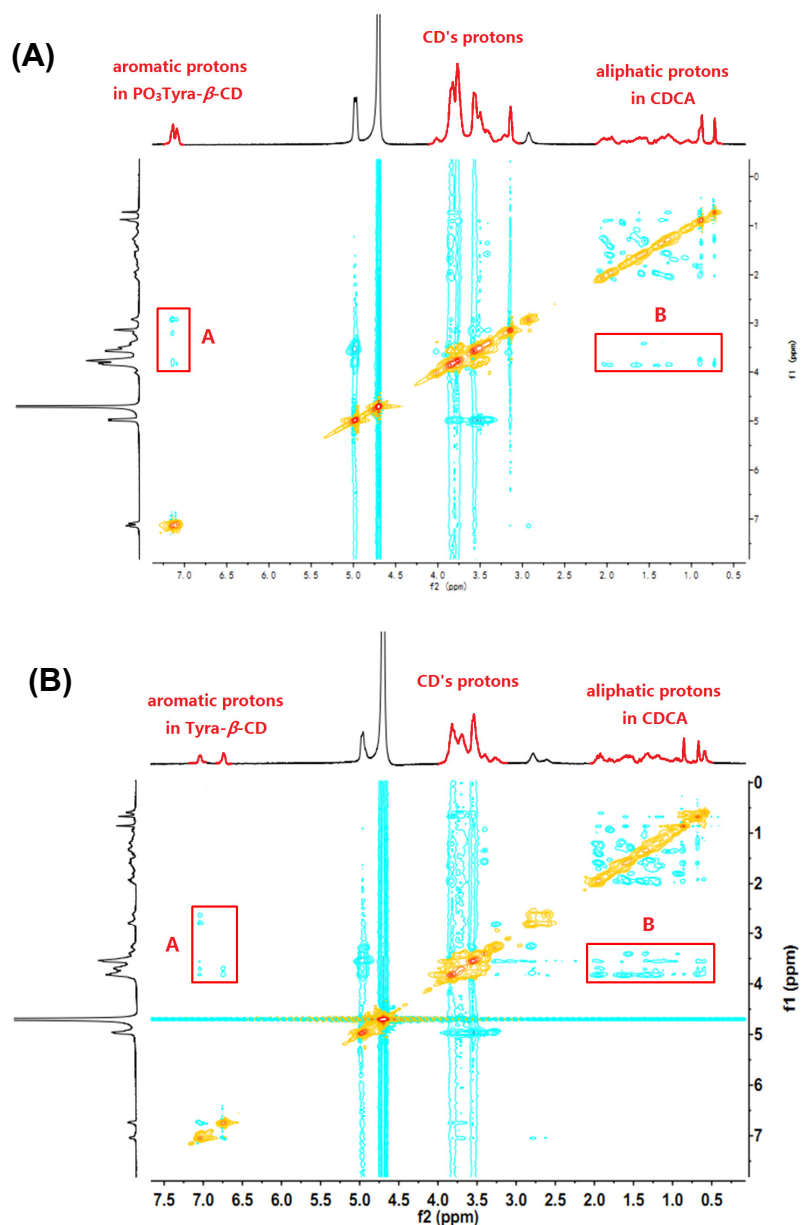


Figure S7. Conformation analyses of inclusion complexation. (A) ^1H ROESY spectrum of (A) CDCA \subset 1 and (B) CDCA \subset 2 complexes after a mixing time of 0.30 s (300 MHz, D₂O, 25 °C). The encircled peaks A were assigned to the NOE correlations between phosphotyramine substituent and β-CD's cavity and encircled peaks B were assigned to the NOE correlations between the steroid skeleton of CDCA and β-CD's cavity, related to Table 1.

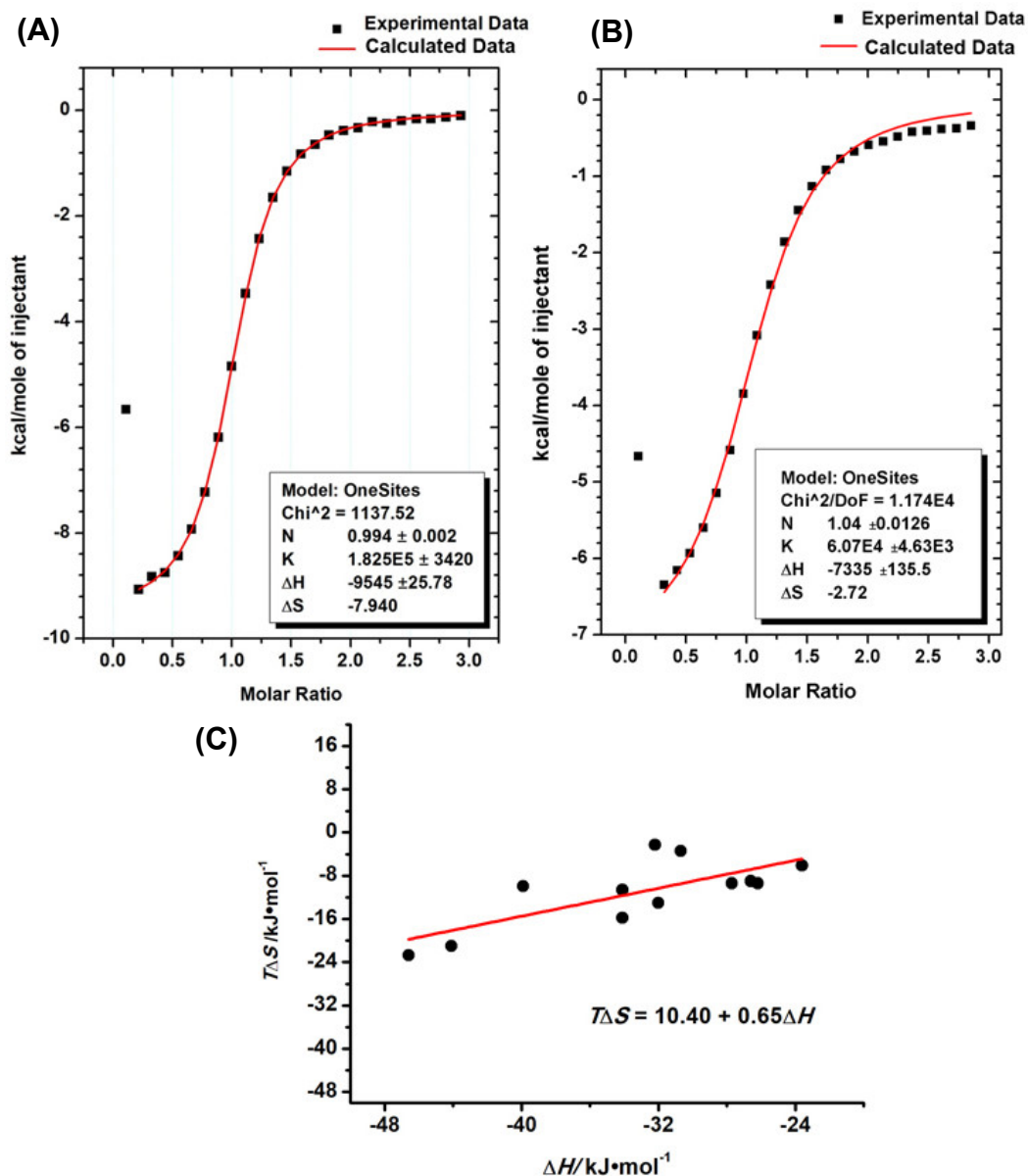


Figure S8. ITC measurements of thermodynamic parameters. Calorimetric titrations for (A) CDCA \subset 2 and (B) CDCA \subset β -CD systems ('Net' heat effect fitted using the 'one set of binding sites' model); (C) Enthalpy-entropy compensation plot for the inclusion complexation of various BAs with hosts β -CD, 1, and 2, related to Table 1.

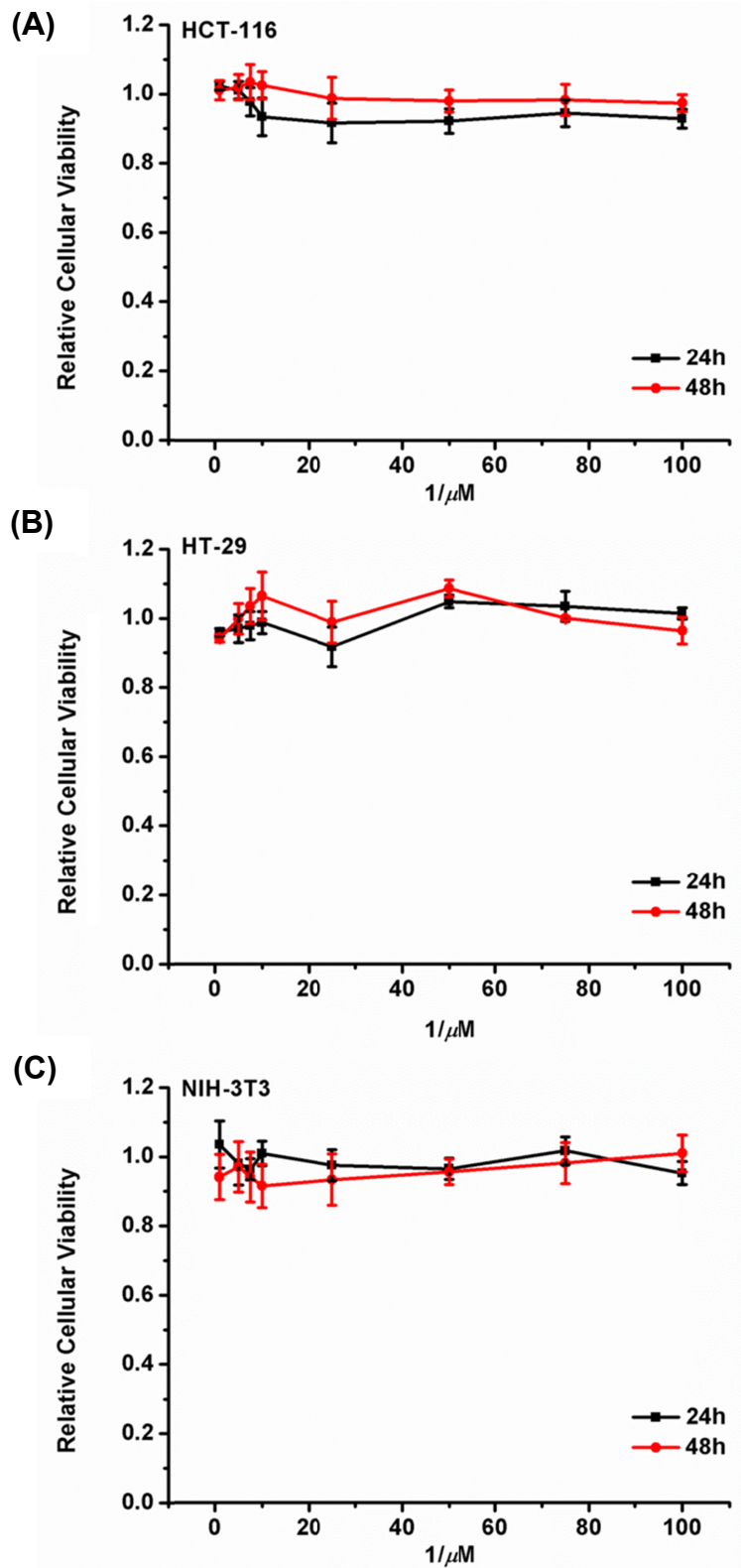


Figure S9. Cytotoxicity assay results of (A) NIH-3T3, (B) HCT-116, and (C) HT-29 cell lines after treatment with host 1 at different concentrations, related to Figure 5.

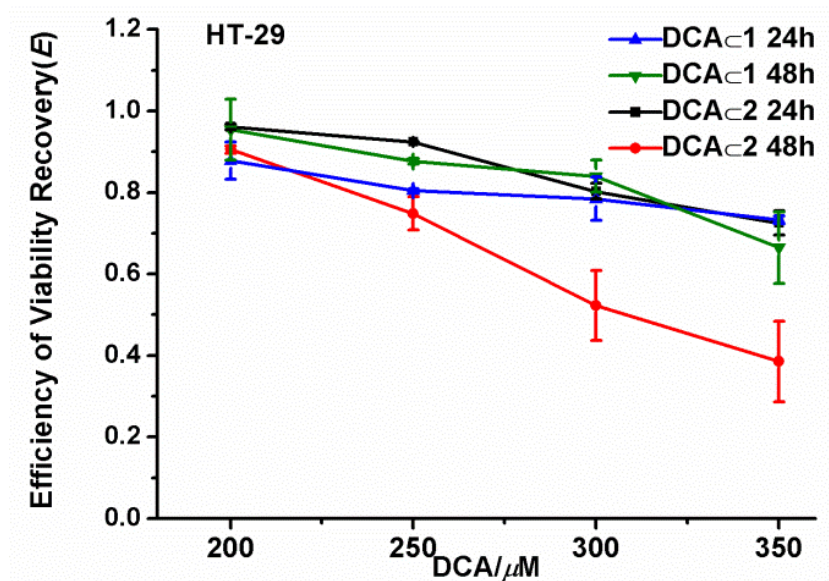


Figure S10. Efficiency of viability recovery (E) of HT-29 cells upon incubation of DCA-bound inclusion complexes after 24 and 48 h, related to Figure 5.

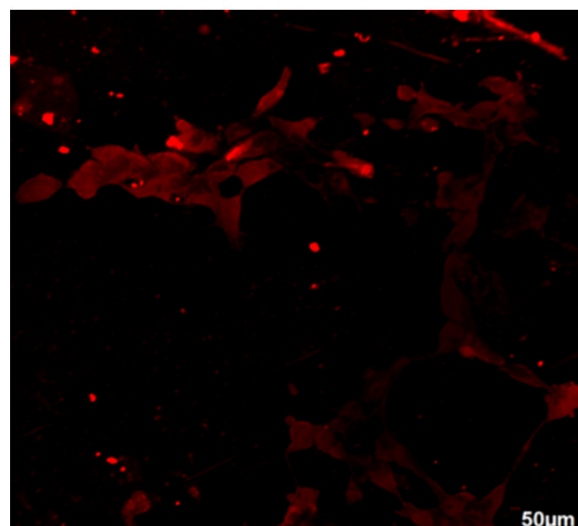


Figure S11. Confocal laser scanning microscopic observation of the release of Ada-Cy5 in NIH-3T3 cells. The scale bar is 50 μ m, related to Figure 5.

Transparent Methods

Materials and Characterization

All chemical reagents were obtained from commercial suppliers unless noted otherwise. The purities of all CDs and derivatives were determined to be > 95% by a combination of ¹H NMR and ¹³C NMR spectroscopy and HRMS. Compound **2** was synthesized according to the reported literature (Zhang et al., 2017). UV/Vis spectra were recorded in a conventional quartz cell (light path 10 mm) on a spectrophotometer equipped with a temperature controller to keep the temperature at 25 °C. Statistical analysis of the data was carried out using the Student's t-test. Differences were considered to be statistically significant if the *p* value was < 0.05.

Synthesis of Phosphotyramine-Modified β-CD **1**

Phosphotyramine was synthesized according to the reported method (White and Backer, 1991). Then a mixture of phosphotyramine (0.4 g) and mono-[6-*O*-(*p*-toluenesulfonyl)]-β-CD (1.0 g) was dissolved in water (15 mL) containing triethanolamine (10 mL), and the resulting mixture was heated at 85 °C for 48 h with stirring under a nitrogen atmosphere. The water was removed by evaporation in vacuo, and the residue was washed with ethanol (200 mL) at least three times to completely remove the excess triethanolamine. Purification of the resulting solid by reversed-phase medium-pressure liquid chromatography with 90:10 (v/v) water/ethanol as the eluent afforded β-CD **1** as a white solid (21%, Figure S1). ¹H NMR (400 MHz, D₂O, ppm): δ 7.15–7.17 (d, 2H, H of phosphotyramine), 5.01–5.03 (m, 7H, H of C-1 of β-CD), 4.07 (s, 2H, H of phosphotyramine), 3.17–3.91 (m, 45H,

H of C-3, C-5, C-6, C-2, and C-4 of β -CD and 3H of phosphotyramine), 2.96 (s, 2H, H of phosphotyramine); ^{13}C NMR (100 MHz, DMSO- d_6 , ppm): δ 128.8, 120.0, 101.9, 81.6, 73.1, 72.4, 72.1, 60.0, 57.6, 49.8; ESI-MS: m/z 1334.4214 $[\text{M} + \text{H}]^+$, 1356.4005 $[\text{M} + \text{Na}]^+$, and 1378.3871 $[\text{M} + \text{K}]^+$.

ITC Measurements

ITC experiments were performed with an isothermal titration microcalorimeter at atmospheric pressure and 25.00 °C in 3% DMSO–phosphate buffer solution (pH 7.2, $I = 0.1$ M) to obtain stability constants (K_S) and other thermodynamic parameters. A solution of bile salts in a 0.250 mL syringe was sequentially injected into a stirring (300 rpm) solution of **1** in the sample cell (1.4227 mL volume). The final concentrations of **1** and bile salts were 0.15 and 2.3 mM, respectively. All the thermodynamic parameters reported in this work were obtained by using the ‘one set of binding sites’ model.

The enthalpy–entropy compensation relationship is given by the following equation (Inoue et al., 1993):

$$T\Delta S = \alpha\Delta H + T\Delta S_0$$

where α and $T\Delta S_0$ are the slope and intercept of a plot of $T\Delta S$ versus ΔH ; α and $T\Delta S_0$ quantitatively reflect the degree of conformational change and the extent of desolvation upon complex formation, respectively.

Preparation of (SLB1@PC Nanoassemblies

A vesicular solution was prepared by means of a film hydration method. In brief, soybean lecithin (7.58 mg) and PEGylated

1,2-distearoyl-sn-glycero-3-phosphoethanolamine (1.68 mg) were dissolved in chloroform (2 mL). The chloroform was then removed by rotary evaporation to afford a thin lipid film. The film was suspended in a HEPES solution of the SLB \subset 1 complex (2 mL), and the suspension was stirred for 0.5 h at 40 °C and then sonicated for 0.1 h at the same temperature ([1] = 1.0 mM with saturated SLB). Lipid vesicles were generated by extruding the resulting suspension through a 220 nm membrane ten times. SLB@PC nanoassemblies were prepared by a similar procedure with a chloroform solution of SLB alone.

In Vitro Release of SLB from SLB@PC and (SLB \subset 1)@PC Nanoassemblies

SLB@PC or (SLB \subset 1)@PC nanoassemblies were incubated with and without ALP to investigate the release rate of SLB. Each sample solution (1.5 mL, [1] = 1.0 mM with saturated SLB) dissolved in HEPES buffer (pH = 7.2, I = 0.02 M) was placed in a dialysis membrane (MW cutoff 3500), which was tightly sealed and immersed in 20 mL of HEPES buffer in a beaker at 37 °C. Release percentage data were collected at selected time intervals after immersion of the dialysis membrane in the beaker. Specifically, a 1-mL sample aliquot was removed from the buffer solution outside the dialysis bag, and the solution was supplemented with 1 mL of fresh buffer solution. The amount of SLB in the aliquot was determined by measuring the UV absorbance at 288 nm.

High-Resolution TEM

High-resolution TEM images of the (SLB \subset 1)@PC nanoassemblies were acquired with a Tecnai 20 high-resolution transmission electron microscope operating at an

accelerating voltage of 200 kV. The sample for TEM measurements was prepared by dropping a solution of (SLB-**1**)@PC nanoassemblies onto a copper grid and then air-drying it.

DLS Measurements

Samples of the (SLB-**1**)@PC nanoassemblies were examined with a laser light scattering spectrometer (BI-200SM) equipped with a digital correlator (TurboCorr) at 636 nm at a scattering angle of 90°. The hydrodynamic diameters of the nanoassemblies were determined from the DLS measurements.

Cell Culture

Mouse embryonic fibroblasts (NIH-3T3) and HT-29 and HCT-116 human colorectal cancer cells were purchased from the Peking Union Medical College Hospital (Beijing, China). The NIH3T3 and HT-29 cells were cultured in a mixture of Dulbecco's modified Eagle's medium (DMEM) and Nutrient Mixture F-12 (DMEM/F-12). The HCT-116 cells were cultured in Iscove's modified Dulbecco's medium supplemented with 10% fetal bovine serum at 37 °C in a humidified 5% CO₂ atmosphere.

Presto Blue Assay

For determination of the cytotoxicity of **1**, 96-well plates were seeded with NIH3T3, HT-29, and HCT-116 cells (5×10^4 cells mL⁻¹, 100 μL per well) for 24 h at 37 °C in 5% CO₂. The cells were then incubated with **1** at concentrations of 10, 50, 75, 100, 250, 500, 750, and 1000 μM for 24 and 48 h, respectively. Relative cellular viabilities were determined by the Presto Blue assay. All data are presented as means ± standard

deviations.

Cell viability experiments were performed using Presto Blue (Bio Source, Invitrogen, UK). Cells were seeded at approximately 5×10^4 cells mL⁻¹ in 96-well plates (100 μ L of medium per well). After 24 h, the exponentially growing cell cultures were treated with the DCA, **1**, and DCA-**1** at DCA concentrations of 200, 250, 300, and 350 μ M. The cells were incubated for 24 and 48 h, respectively. All data are presented as means \pm standard deviations. The efficiency of viability recovery (E) was defined as $E = V_{\text{complex}}/V_{\text{host}}$, where V_{complex} and V_{host} are the relative cell viabilities in the presence of the host compound (**1** or **2**) with and without DCA, respectively.

Confocal Laser Scanning Microscopy

To image the liposomes, we first cultured NIH3T3 cells in DMEM supplemented with 10% fetal bovine serum at 37 °C in humidified air containing 5% CO₂. Then 6-well plates were seeded with NIH3T3 cells in 1.0 mL of complete DMEM. After incubation for 24 h, the cells were treated with a solution of (Ada-Cy5-**1**)@PC ([**1**] = [Ada-Cy5] = 1.0 mM). After 6 h, the culture medium was removed, and the cells were washed twice with phosphate buffered saline and fixed in 4% paraformaldehyde. The cover slip was removed from the 6-well plate, and a glass slide was mounted on the cover slip and fixed. Images were obtained with a confocal laser scanning microscope (Olympus FV₁₀₀₀) at an excitation wavelength at 649 nm.

In Vivo Experiments in a Murine Model of Liver Injury

To establish an appropriate murine model, BALB/c female mice were intraperitoneally injected with CCl₄ to induce acute liver injury (Hermenean et al.,

2014). The mice were housed at a constant temperature (23 ± 1 °C) and controlled humidity (45–65%) under a standard 12-h light/dark cycle. Animals fasted for at least 2 h prior to the experiments. Solutions of **1**, SLB, free PC, and (SLB**1**)@PC were prepared in phosphate buffered saline (pH 7.2). Mice were randomly divided into four groups ($n = 3$ in each group). Each mouse was intraperitoneally injected with 400 μ L of one of the test solutions at 1 and 6 h after injection of the CCl₄. Then variations in the plasma levels of ALP, ALT, and TBA were measured 20 h after treatment with CCl₄. All treated mice were maintained under the same experimental conditions, and no abnormal behavior or symptoms were observed. Blood samples were collected by removal of the eyeball, and then the mice were killed by cervical dislocation. The collected blood samples were centrifuged at 1500 rpm for 5 min to obtain the serum. The serum was analyzed with ALP, cereal third transaminase (ALT), and TBA kits according to the manufacturers' instructions. All mouse experiments were approved by the Institutional Animal Care and Use Committee of Nankai University. All mice had free access to food and water throughout the experiments.

Supplemental References

Zhang, Y.-M., Xu, X., Yu, Q., Liu, Y.-H., Zhang, H.-Y., Chen, L.-X., and Liu, Y. (2017). Reversing the Cytotoxicity of Bile Acids by Supramolecular Encapsulation. *J. Med. Chem.* *60*, 3266–3274.

White, M.F., and Backer, J.M. (1991). Preparation and use of anti-phosphotyrosine antibodies to study structure and function of insulin receptors. *Methods Enzymol.* *201*, 65–79.

Inoue, Y., Liu, Y., Tong, L.-H., Shen, B.-J., and Jin, D.-S. (1993). Calorimetric titration of inclusion complexation with modified β -cyclodextrins. Enthalpy-entropy compensation in host–guest complexation: from ionophore to cyclodextrin and cyclophane. *J. Am. Chem. Soc.* *115*, 10637–10644.

Hermenean, A., Ardelean, A., Stan, M., Hadaruga, N., Mihali, C.-V., Costache, M., and Dinischiotu, A. (2014). Antioxidant and hepatoprotective effects of naringenin and its β -cyclodextrin formulation in mice intoxicated with carbon tetrachloride: A comparative study. *J. Med. Food* *17*, 670–677.